Study on the Microtremor Horizontal-to-Vertical Spectral Ratio Based on Response Spectra

Yuxin Han[1], Yan-Gang Zhao[1], and Haizhong Zhang[*2]

ABSTRACT

The microtremor horizontal-to-vertical spectral ratio (MHVSR) has been widely used to evaluate site effects due to its simplicity, high efficiency, and low cost. Commonly, MHVSR is calculated based on the Fourier amplitude spectra (FAS) of microtremor records, which requires a smoothing procedure to clearly observe the overall shape of the curves. However, MHVSR—particularly its amplitude—can be affected by the choice of smoothing technique. A previous study has recommended using response spectra instead of FAS for the MHVSR evaluation to eliminate efforts for smoothing and to obtain unique MHVSR results, but the applicability has not been systematically explored. In this study, a theoretical analysis of the response-spectra-based MHVSR (RMHVSR) is first conducted based on random vibration theory. In addition, the RMHVSR is explored based on microtremor records observed at 104 sites in Japan and site borehole data. Specifically, MHVSRs calculated from response spectra are systematically compared with those derived from FAS. It is found that the MHVSR based on response spectra is less sensitive to long-period signals compared with that based on FAS, making it less susceptible to long-period noise, such as that caused by wind. When the site fundamental period is short, the shapes of the two MHVSRs are highly similar, with their predominant periods aligning, though the peak amplitude based on response spectra is lower. In this case, RMHVSR is effective. However, when the site fundamental period is longer than around 0.8 s, the peak corresponding to the site fundamental period may be smoothed out when using response spectra, leading to inaccurate evaluations.

KEY POINTS

- The response-spectra-based microtremor horizontal-to-vertical spectral ratio (RMHVSR) was theoretically explored using random vibration theory.
- The RMHVSR is less sensitive to long-period signals.
- When the site fundamental period is short, MHVSR based on response and Fourier spectra exhibit similar shapes.

Supplemental Material

INTRODUCTION

The microtremor horizontal-to-vertical spectral ratio (MHVSR) is a widely used tool for estimating site effects (Bard, 1999; Delgado *et al.*, 2000; Fäh *et al.*, 2003; Scherbaum *et al.*, 2003; Parolai *et al.*, 2005; Tebbouche *et al.*, 2017; Zare *et al.*, 2017). The MHVSR is typically calculated by dividing the geometric mean of the Fourier amplitude spectra (FAS) of the two horizontal components by the FAS of the vertical component. In the calculation process, the FAS usually needs to be smoothed to distinguish smooth spectral peaks that correspond to site-effect characteristics from many peaks present in unsmoothed spectra (Zhao *et al.*, 2006). However, various techniques are available for FAS smoothing, and the MHVSR—particularly its amplitude—can be influenced by the choice of smoothing technique (Hinzen *et al.*, 2004; D'Amico *et al.*, 2008; Haghshenas *et al.*, 2008).

Many smoothing windows have been proposed for smoothing FAS, with the Parzen window and Konno–Ohmachi (KO) window being the most commonly used. Konno and Ohmachi (1998) pointed out that the width of the Parzen window increases with the period on a logarithmic axis. This leads to varied smoothing of the MHVSR peak height depending on the predominant period, resulting in smoother and lower peaks for longer periods. Konno and Ohmachi (1998) proposed a logarithmic smoothing window, known as the KO window, width for which remains constant on a logarithmic axis. Nevertheless, Senna *et al.* (2008) argued that the binomial smoothing filter developed by Marchand and Marmet (1983) outperforms both the Parzen and KO windows. Moreover, other smoothing

1. College of Architecture and Civil Engineering, Beijing University of Technology, Beijing, China; 2. Eco-Science Course, Faculty of Agriculture, Yamagata University, Yamagata, Japan

*Corresponding author: zhang@tds1.tr.yamagata-u.ac.jp

Cite this article as Han, Y., Y.-G. Zhao, and H. Zhang (2025). Study on the Microtremor Horizontal-to-Vertical Spectral Ratio Based on Response Spectra, *Bull. Seismol. Soc. Am.* **XX**, 1–14, doi: 10.1785/0120250019

windows, such as the Hanning window (Parolai *et al.*, 2002), the triangle window (Gosar and Lenart, 2010; Rupar and Gosar, 2020), the Blankman window (Miura *et al.*, 2023), the moving average operator (Diagourtas *et al.*, 2001), and the sliding window (Delgado *et al.*, 2000), are also widely used for FAS smoothing in the MHVSR calculations.

In addition, even for the same window, different researchers adopt varying bandwidth coefficients, which can also lead to variations in the MHVSR results (Bao *et al.*, 2018; Yao *et al.*, 2019; Molnar *et al.*, 2022). For example, although Matsushima *et al.* (2014), Kawase *et al.* (2019), and Pan *et al.* (2022, 2024) all used the Parzen window, Matsushima *et al.* (2014) and Kawase *et al.* (2019) selected a bandwidth coefficient of b = 0.1 Hz, whereas Pan *et al.* (2022, 2024) used b = 0.3 Hz. Similarly, many researchers applied the KO window (Massa *et al.*, 2017; Wu *et al.*, 2017; Brax *et al.*, 2018; Mascandola *et al.*, 2019; Zhu *et al.*, 2020; Chieppa *et al.*, 2023; Stolte *et al.*, 2023), with some choosing the bandwidth coefficient b as 20, others using b = 40, b = 50, or b = 60. In addition, Bindi *et al.* (2001) and Parolai *et al.* (2002) both applied the Hanning window. Bindi *et al.* (2001) used a 0.5 Hz half-width, whereas Parolai *et al.* (2002) employed a 28% bandwidth. Currently, the choice of smoothing window and corresponding bandwidth coefficients is often subjective (Cox *et al.*, 2020; Araque-Perez, 2024), and the MHVSR can be influenced by this choice.

Recently, Laouami (2020) proposed calculating MHVSR based on response spectra, which eliminates the need for smoothing and yields unique MHVSR results. Laouami (2020) applied the response-spectra-based MHVSR (RMHVSR) method for site classification corresponding to the four standard soil classes (rock, soft rock, stiff soil, and soft soil) defined in Eurocode-8. However, the applicability of the RMHVSR has not been systematically explored. This study aims to clarify its applicability from both theoretical and statistical perspectives. The remainder of this study is organized as follows. First, the applicability of the RMHVSR is theoretically analyzed based on random vibration theory (RVT). Subsequently, microtremor records observed from 104 sites with borehole information in Japan are presented. Based on these microtremor records and the borehole information, the RMHVSR is then systematically explored. Finally, the main conclusions of this study are summarized.

THEORETICAL ANALYSIS OF THE RMHVSR

To assess the applicability of the RMHVSR, a theoretical analysis of RMHVSR is conducted in this section. Han *et al.* (2024) derived a theoretical equation for the response-spectra-based horizontal-to-vertical spectral ratio, RHVSR($\bar{\omega}$,h_0), for earthquake ground motions based on RVT, which is expressed as

$$\mathrm{RHVSR}(\bar{\omega},h_0) = \sqrt{\int_0^\infty U_p(\omega,\bar{\omega},h_0)|\mathrm{FHVSR}(\omega)|^2 d\omega}, \quad (1)$$

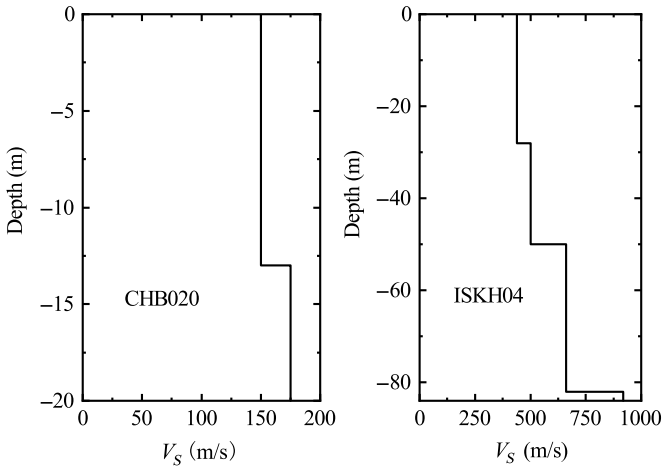

Figure 1. V_S profiles of the two sites.

in which $\overline{\omega}$ and h_0 are the circular frequency and damping ratio of the single-degree-of-freedom (SDOF) oscillator, respectively, and ω is the circular frequency of the FAS. FHVSR(ω) represents the horizontal-to-vertical spectral ratio calculated based on FAS, and $U_p(\omega,\bar{\omega},h_0)$ is expressed as

$$U_p(\omega,\bar{\omega},h_0) = \frac{F_V^2(\omega)|H_0(\omega,\bar{\omega},h_0)|^2}{\int_0^\infty F_V^2(\omega)|H_0(\omega,\bar{\omega},h_0)|^2 d\omega}, \quad (2)$$

in which $F_V(\omega)$ is the FAS of vertical ground motion, and $H_0(\omega,\bar{\omega},h_0)$ is the SDOF transfer function, which is expressed as

$$|H_0(\omega,\bar{\omega},h_0)| = \frac{\bar{\omega}^2}{\sqrt{(2h_0\omega\bar{\omega})^2 + (\omega^2 - \bar{\omega}^2)^2}}. \quad (3)$$

Although equation (1) was derived for earthquake ground motion, it can be easily inferred that it is also valid for microtremor records. To verify this inference, microtremors were observed on two sites in strong motion seismograph networks (Kyoshin net, Kiban–Kyoshin network) (Okada *et al.*, 2004; Aoi *et al.*, 2011). The station codes for the two sites are CHB020 and ISKH04, respectively. Table 1 details information on the two sites, including the coordinates, shear-wave velocity (V_S) of the surface layer, S, and the time-averaged V_S in the upper 30 m, V_{S30}. Figure 1 shows the V_S profiles of the two sites.

TABLE 1
Information of the Selected Sites

Station ID	Coordinates (°)		Site Conditions	
Code	Longitude	Latitude	S (m/s)	V_{S30} (m/s)
CHB020	140.1022 E	35.1155 N	150	134.4
ISKH04	136.7176 E	37.1902 N	440	443.5

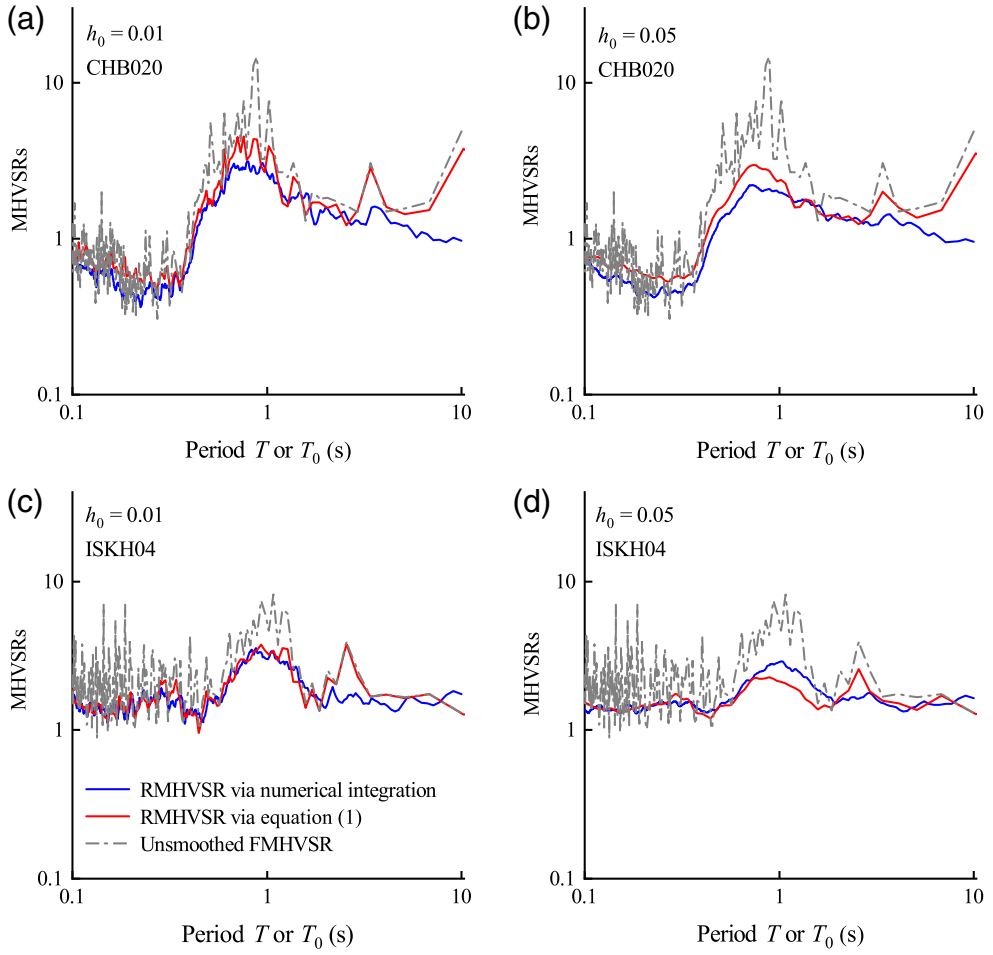

Figure 2. Comparison of the response-spectra-based microtremor horizontal-to-vertical spectral ratio (RMHVSR) results obtained via equation (1) and the direct numerical integration. Each row (a,b) and (c,d) shows the results for different sites: CHB020 and ISKH04. Each column (a,c) and (b,d) shows the results for different damping ratios h_0: 0.01 and 0.05. The color version of this figure is available only in the electronic edition.

Then, the RMHVSR is calculated using equation (1) from the traditional FAS-based MHVSR (FMHVSR), which is determined by dividing the square root of the product of the FAS of the two horizontal components by the FAS of the vertical component of the microtremor records. The RMHVSRs obtained using equation (1) are compared with those calculated based on the response spectra of the three components derived from direct numerical integration. Here, two damping ratios, 0.01 and 0.05, are considered in the calculations. The obtained results for the two sites with different damping ratios are shown in Figure 2. For reference, unsmoothed FMHVSR results are also presented in Figure 2. It is found that the RMHVSRs calculated using equation (1) are very similar to those derived from direct numerical integration. Although the inconsistency of RMHVSRs from equation (1) and direct numerical integration may increase slightly with a higher damping ratio (e.g., Fig. 2b,d), the peaks and predominant periods of both methods remain similar. These findings are highly consistent with the previous studies based on earthquake ground motions, verifying the accuracy of equation (1) and its applicability to microtremor analysis.

The theoretical properties of RMHVSR can be systematically explored based on equation (1). It is observed that equation (1) describes a smoothing process of a function. FMHVSR is a function to be smoothed, $U_p(\omega,\overline{\omega},h_0)$ is the smoothing window, and RMHVSR is the result obtained after smoothing. The term $U_p(\omega,\overline{\omega},h_0)$ satisfies the conditions required for smoothing window (i.e., $\int_0^{+\infty} U_p(\omega,\overline{\omega},h_0)d\omega = 1$). The smoothing process for each oscillator period T_0 ($T_0 = 2\pi/\overline{\omega}$) involves a weighted average calculation, in which the smoothing window acts as a weighting function. Specifically, the RMHVSR value at each T_0 is equal to the weighted average of the square of FMHVSR from zero to infinity at the circular frequency ω, and the $U_p(\omega,\overline{\omega},h_0)$ value at ω represents the weight for the FMHVSR values at the same circular frequency. To calculate RMHVSR for different oscillator periods, the smoothing window $U_p(\omega,\overline{\omega},h_0)$ needs to be shifted to the target T_0. Figure 2 offers a preliminary understanding of the smoothing process described in equation (1), demonstrating that the RMHVSR represents a smoothed form of the FMHVSR, as evident from the overall shapes of the curves.

To further investigate the smoothing properties, the smoothing window $U_p(\omega,\overline{\omega},h_0)$ is analyzed. As evident from equation (2), $U_p(\omega,\overline{\omega},h_0)$ is determined by the oscillator transfer function $H_0(\omega,\overline{\omega},h_0)$ and the FAS of the microtremor vertical component. To illustrate their properties, representative results for $H_0(\omega,\overline{\omega},h_0)$ and the FAS of the microtremor vertical component are shown in Figures 3 and 4, respectively. In Figure 3, three oscillator periods T_0 (0.5, 2, and 4 s) are considered with $h_0 = 0.01$ and 0.05, respectively. In Figure 4, the FAS of the vertical component of the microtremor is calculated for two records from two sites. As shown in Figure 3, regardless of the shift in the oscillator period T_0, $H_0(\omega,\overline{\omega},h_0)$ exhibits a narrowband peak at the oscillator period T_0 and decreases rapidly to

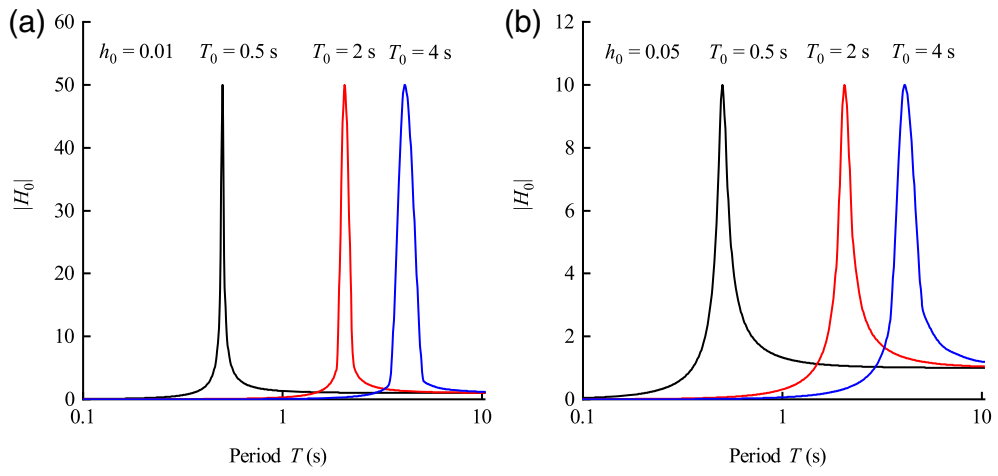

Figure 3. Variation of the transfer function $H_0(\omega,\bar{\omega},h_0)$ with the oscillator period considering two damping ratios (a) $h_0 = 0.01$ and (b) $h_0 = 0.05$. The color version of this figure is available only in the electronic edition.

zero and unity as the period decreases and increases, respectively. Figure 4 illustrates that the overall shape of the FAS of the microtremor vertical component is much flatter compared to $H_0(\omega,\overline{\omega},h_0)$. Therefore, the shape of $U_p(\omega,\overline{\omega},h_0)$ is determined by $H_0(\omega,\overline{\omega},h_0)$, and the properties of $H_0(\omega,\overline{\omega},h_0)$ provides insight into the characteristics of $U_p(\omega,\overline{\omega},h_0)$. Because $H_0(\omega,\overline{\omega},h_0)$ has a sharp peak around T_0, the shape of $U_p(\omega,\overline{\omega},h_0)$ also typically exhibits a sharp peak around T_0. Furthermore, as the oscillator period T_0 increases, the bandwidth of the $H_0(\omega,\overline{\omega},h_0)$ widens on a logarithmic axis. Consequently, the bandwidth of the smoothing window $U_p(\omega,\overline{\omega},h_0)$ also becomes progressively wider on a logarithmic axis, as illustrated in Figure 5.

The theoretical properties of RMHVSR can be inferred from the characteristics of the smoothing window $U_p(\omega,\overline{\omega},h_0)$. Because RMHVSR represents the weighted average related to FMHVSR, and $U_p(\omega,\overline{\omega},h_0)$ has a sharp peak around T_0, indicating that the weights are concentrated near the oscillator period T_0, the shapes of RMHVSR and FMHVSR are similar. This observation is also supported by Figure 2. However, as $U_p(\omega,\overline{\omega},h_0)$ widens with increasing T_0 on the logarithmic axis, it follows that a wider bandwidth at T_0 involves more data in the weighted average calculation, resulting in a smoother RMHVSR and lower peaks as the period increases. Similar to the Parzen window, this property enhances smoothness and reduces sensitivity to long-period signals. This property of RMHVSR has both advantages and disadvantages. Because the peaks of MHVSR at a very long period are often associated with unknown sources unrelated to site effects, such as wind influences (Sesame, 2004; Laouami, 2020), the property of RMHVSR makes it less susceptible to long-period noise. However, if a source related to site effects causes a peak at a long

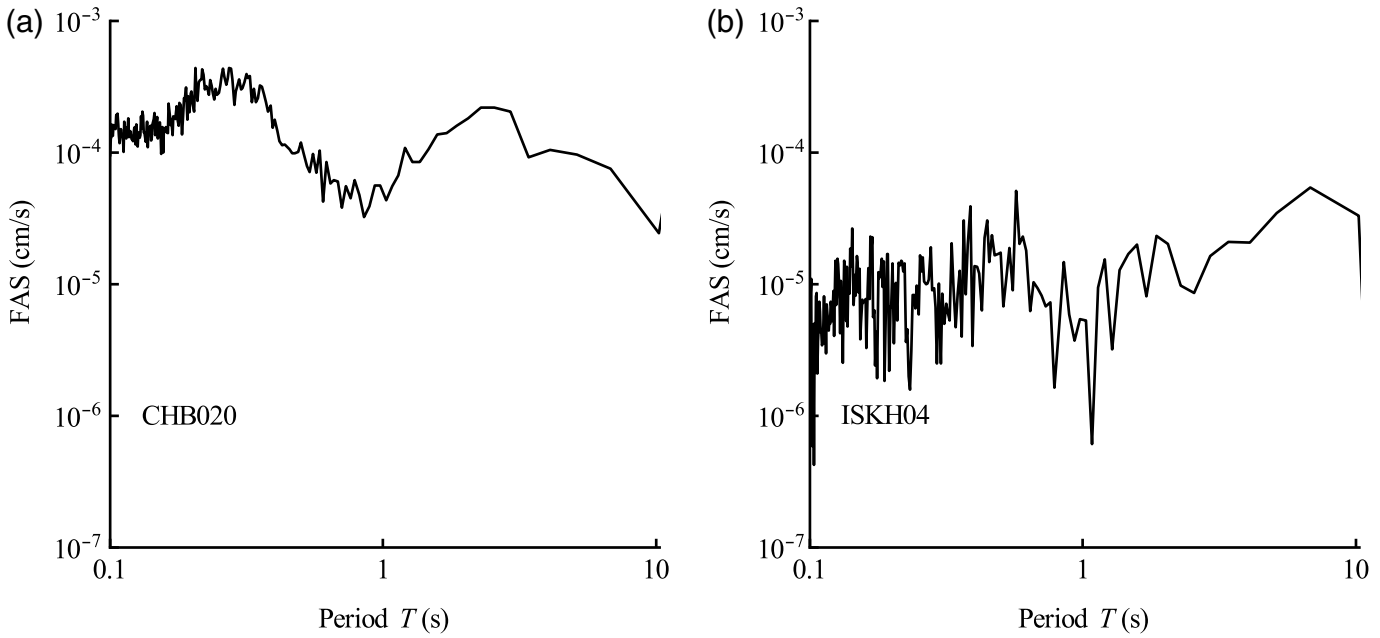

Figure 4. The Fourier amplitude spectra (FAS) of the microtremor vertical component for (a) site CHB020 and (b) site ISKH04.

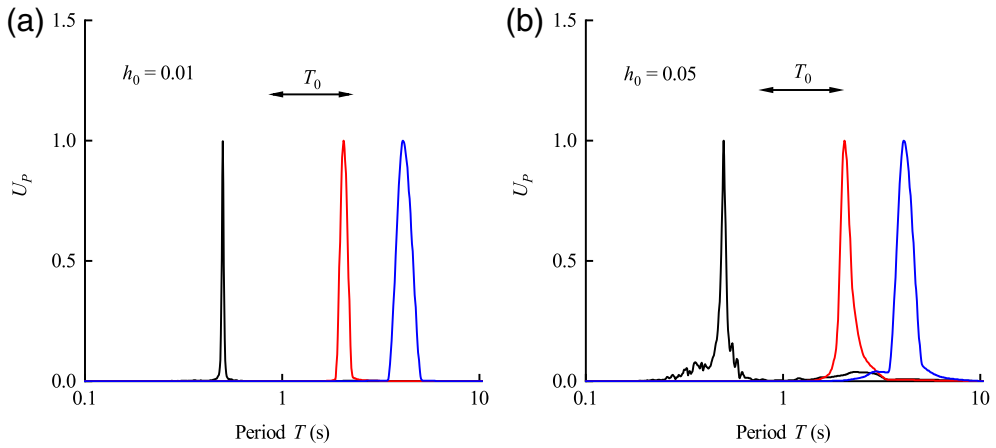

Figure 5. Variation of the smoothing window $U_p(\omega,\tilde{\omega},h_0)$ with the oscillator period considering two damping ratios (a) $h_0 = 0.01$ and (b) $h_0 = 0.05$. The color version of this figure is available only in the electronic edition.

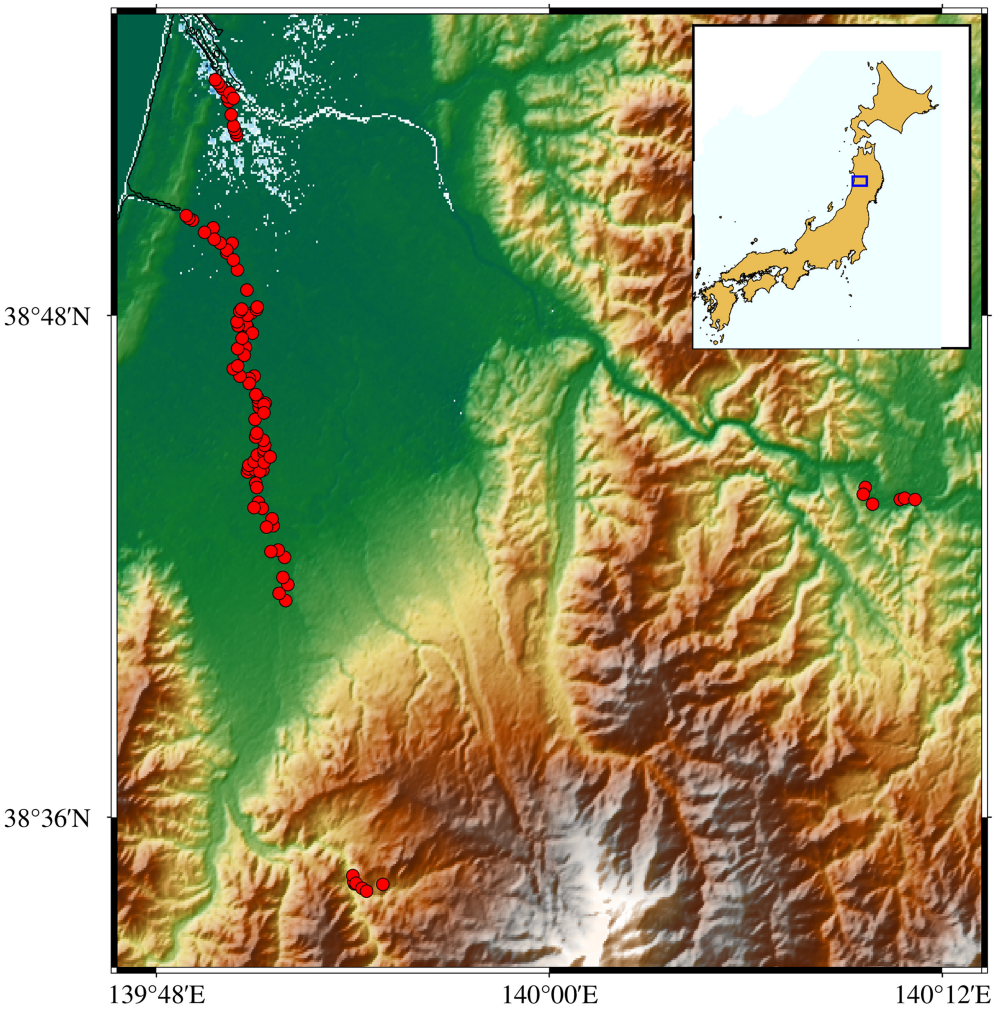

Figure 6. Distribution of microtremor observation sites in Japan. The top inset figure shows Japan's entire territory, with the blue rectangle indicating the observation area's location. The color version of this figure is available only in the electronic edition.

period, the excessive smoothing of RMHVSR may result in inaccuracies.

MICROTREMOR MEASUREMENT

To further investigate the properties of RMHVSR, microtremors were observed at 104 sites in Japan, most of which have corresponding borehole data. The sites were sequentially numbered from number 1 to 104. The McSEIS-AT 3CH data logger, developed by OYO Corporation, Japan, was used for the observations. The sensor (MODEL-1135) with a natural period of 2 Hz was used as a seismometer (PS-2B manufactured by SUNFULL) (Suzuki *et al.*, 2019). The sites were recorded for 20 min in continuous time in the east–west (EW), the north–south (NS), and the vertical (V) directions at a rate of 250 samples per second. To guarantee records reliability, effective coupling between the instrument and the ground was established before records collection. Specifically, for hard ground surfaces free of grass, stones, or other obstructions, the instrument was placed directly on the ground. In cases involving soft soil or ground covered by vegetation, the sensor was securely anchored by inserting spikes into the soil. Figure 6 shows the study area in Japan where the microtremor measurements were performed. To obtain data from various sites, observations were conducted not only in plains, but also in mountainous regions. Figure 7 shows the standard penetration test blow count (hereafter called *N*-value) profiles for some representative sites, obtained from the National Geo-Information

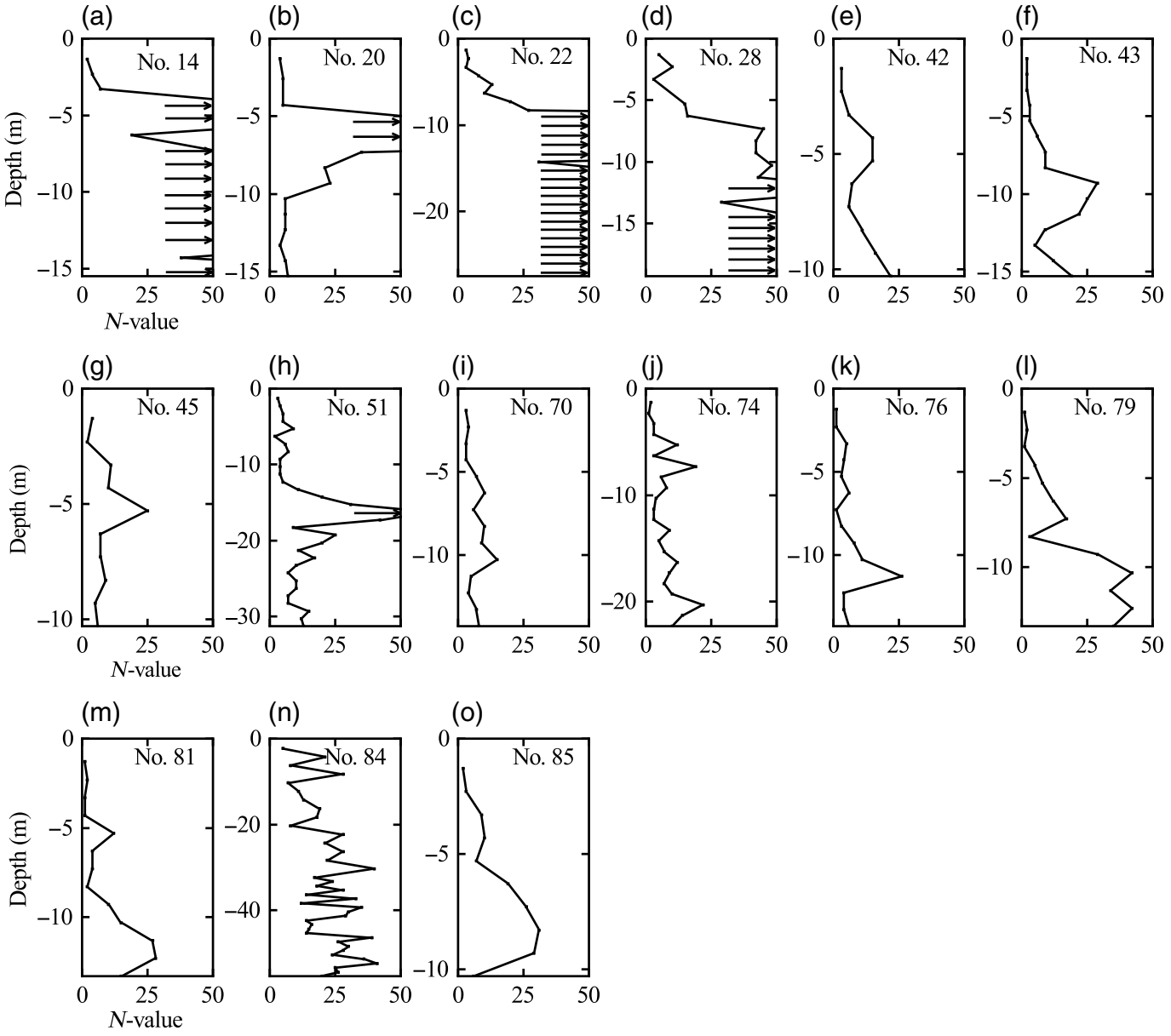

Figure 7. Panels (a–o) represent the *N*-value profiles corresponding to the site number in each figure, respectively. For other sites, see Figure S7.

Center (see Data and Resources). Profiles for additional sites are provided in Figure S7, available in the supplemental material to this article. Note that seven sites lacked *N*-value data. The numbers in the figure correspond to site codes, with arrows indicating depths where the *N*-value exceeds 50. In addition, Figure 8 presents average wind speed data recorded by the Japan Meteorological Agency (see Data and Resources) during the measurement period, providing data for analyzing wind-induced noise.

ANALYSIS OF THE RMHVSR BASED ON REAL OBSERVATIONS

To systematically explore the applicability of RMHVSR, it was calculated using the microtremor records in the previous section and compared with FMHVSR. A baseline correction was applied to each component of the microtremor records using the least-squares method to remove noise, without employing any additional filtering. Eight nonoverlapping stationary recording segments of 20.48 s were selected from each microtremor record. The RMHVSR and FMHVSR of each segment were calculated by dividing the geometric mean of the two horizontal components by the vertical component. The average MHVSR from the eight segments was used as the estimated result. For response spectra calculations, the recorded microtremor velocities were converted to accelerations, and two damping ratios ($h_0 = 0.01$ and $h_0 = 0.05$) were considered. To smooth the FAS, two windows were applied: a Parzen window with a bandwidth coefficient of b = 0.5 Hz, and a KO window with a bandwidth coefficient of b = 20.

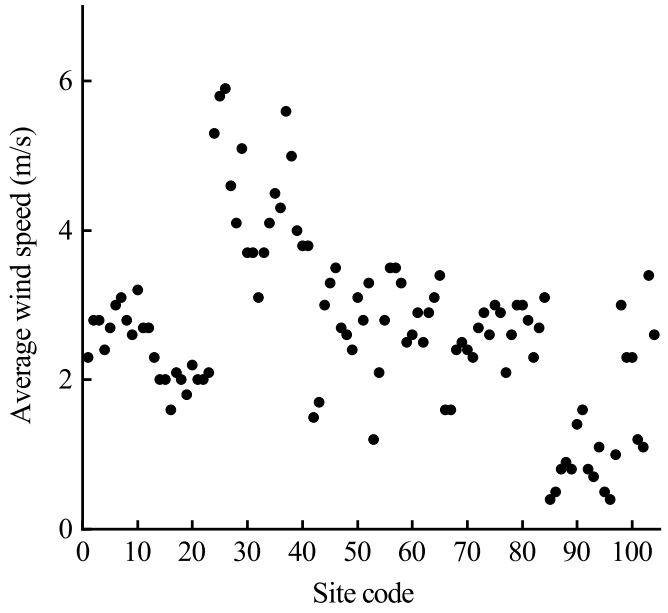

Figure 8. Average wind speed data during measurement. For the maximum wind speed data recorded during measurement, see Figure S8.

A preliminary analysis of FMHVSR results from 104 sites revealed that 36 sites have peak amplitudes of the FMHVSR curve less than 2, which fails to meet the SESAME (2004) criterion for a clear FMHVSR peak. Therefore, these sites are excluded from further analysis in this study. The representative RMHVSR and FMHVSR results for the remaining 68 sites are shown in Figures 9 and 10, with additional results provided in Figure S9. To systematically explore the applicability of RMHVSR for estimating the predominant period and peak amplitude, the RMHVSR results are compared with those of FMHVSR, as shown in Figures 11 and 12. For the determination of the predominant period and peak amplitude from RMHVSR and FMHVSR curves, when the curve has only one peak, the corresponding period is treated as the predominant period, and its amplitude is treated as peak amplitude. When the curve has two peaks, the one with a larger amplitude is used to calculate the predominant period and peak amplitude. In addition, because the conclusions for damping ratios of 0.01 and 0.05 are similar, only RMHVSR results with a damping ratio of 0.01 are shown in Figures 11 and 12. Figure 11a,b compares the predominant period and peak amplitude of RMHVSR with those of FMHVSR based on the KO window, respectively. Similarly, Figure 12a,b compares the predominant period and peak amplitude of RMHVSR with those of FMHVSR based on the Parzen window. As shown in Figures 11a and 12a, for FMHVSR with short predominant periods (~50 sites), the predominant periods of RMHVSR and FMHVSR exhibit strong correlations. However, for FMHVSR with long predominant periods (greater than around 0.8 s) (~15 sites), the predominant periods of RMHVSR and FMHVSR show poor correlation. For these cases, the predominant periods of RMHVSR are generally shorter than those of FMHVSR. In addition, Figures 11b and 12b indicate a strong correlation between RMHVSR and FMHVSR in terms of peak amplitude. To evaluate the influence of smoothing windows on FMHVSR, results obtained using two different windows are compared in Figure 13a,b. The findings demonstrate a strong correlation between the two smoothing techniques, regardless of the predominant period or peak amplitude. To further assess the applicability of RMHVSR, the results from the 68 sites were categorized into two types. Type I curves exhibit high consistency between predominant periods of RMHVSR and FMHVSR, whereas type II curves show poor consistency between them.

Figure 9 presents the type I curves, encompassing 11 representative sites. The results for these sites indicate that the shapes of the MHVSR curves derived from the two spectra are similar, with the maximum values occurring at the same periods, regardless of the damping ratio used for the response spectra or the smoothing technique applied to the FAS. In addition, the peak amplitudes of the RMHVSR curves are consistently lower than those of the FMHVSR curves. These observations further support the theoretical deduction outlined in the previous section—namely, that RMHVSR represents a smoothed form of FMHVSR. Moreover, the predominant periods of these curves are generally short. However, RMHVSR exhibits certain anomalous behaviors at specific sites, characterized by the upward warping of the curve at long periods. This behavior is inconsistent with FMHVSR, as illustrated in Figure 9a,e,g. The underlying cause of this phenomenon is that $H_0(\omega,\bar{\omega},h_0)$ does not approach zero at long periods, as shown in Figure 3. Consequently, if unsmoothed FMHVSR displays abnormally large values at long periods, these values are incorporated into the weighted average calculation, causing the RMHVSR curve to upward warping at long periods. For RMHVSR curves with different damping ratios, the shapes remain highly consistent, with the maximum value always occurring at the same periods. Furthermore, as the damping ratio increases, the RMHVSR curves become smoother and exhibit lower amplitudes. This behavior can be attributed to the increased bandwidth of the smoothing window $U_p(\omega,\overline{\omega},h_0)$ as the damping ratio increases, as shown in Figure 5. The broader bandwidth enhances the smoothing effect, resulting in a smoother overall shape of the RMHVSR curves.

Figure 10 shows the type II of curves, comprising 16 sites. A comparison of these results reveals that the MHVSR curves derived from the two spectra differ in shape, with their maximum values occurring at different periods. Specifically, for FMHVSR curves with a single prominent peak corresponding to a long predominant period, such as those shown in Figure 10h,i,n,p, the RMHVSR curve typically lacks a distinct peak and appears relatively flat at longer periods. For FMHVSR curves with two prominent peaks, the maximum peak occurs at a longer period, as exemplified in Figure 10b–d,k,o. In contrast, the RMHVSR curve generally exhibits only a single

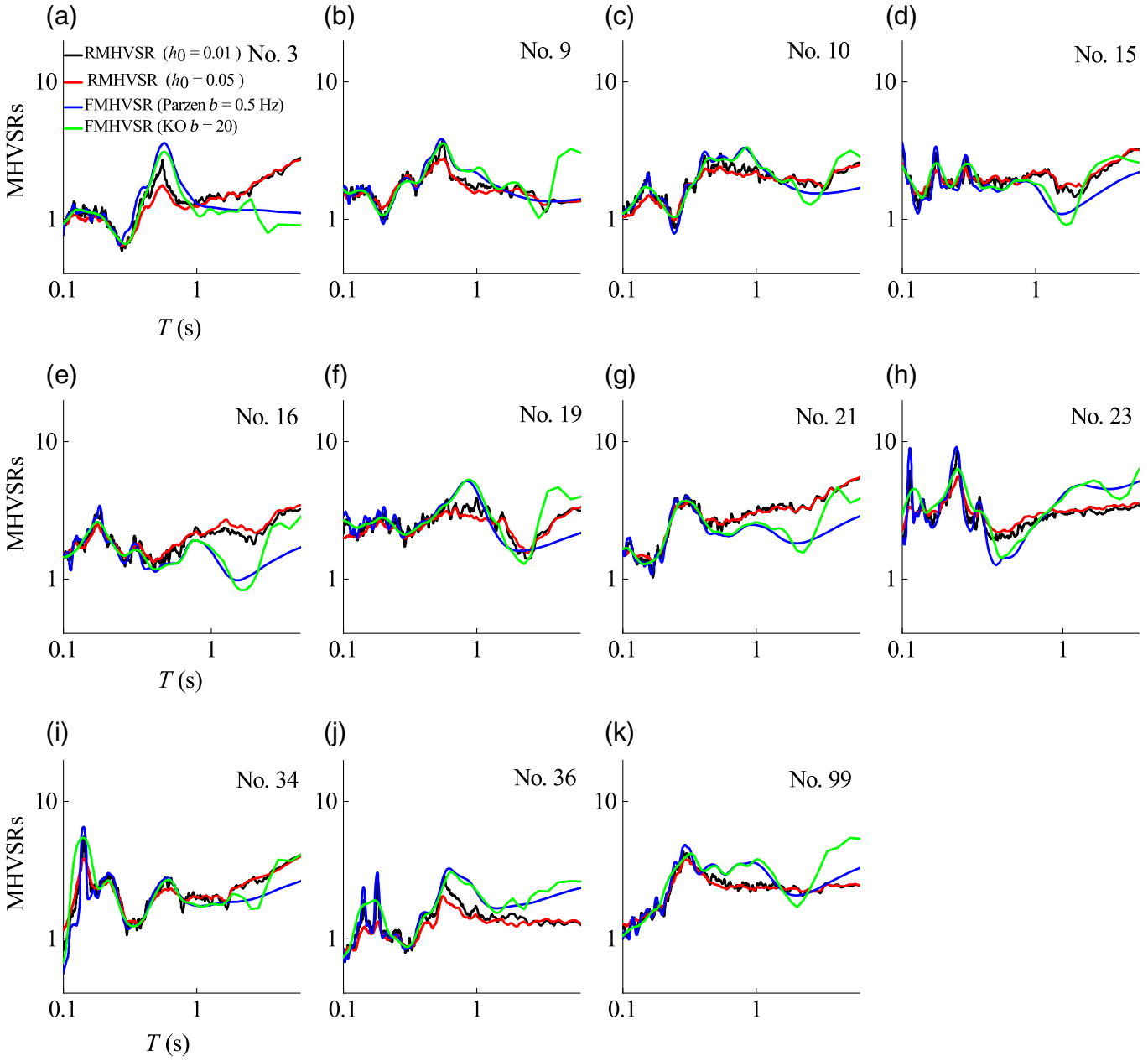

Figure 9. Comparison of RMHVSR and FAS-based MHVSR (FMHVSR) results demonstrating high consistency, considering damping ratios of 0.01 and 0.05. For the FMHVSR results, FAS is smoothed by the Parzen window with b = 0.5 Hz and KO window with b = 20. Panels (a–k) represent the results corresponding to the site number in each figure, respectively. For results of other sites, see Figure S9. The color version of this figure is available only in the electronic edition.

peak at a shorter predominant period. Overall, when FMHVSR shows a clear peak at a long period, RMHVSR consistently lacks a corresponding peak at that period. This discrepancy is a result of the inherent properties of RMHVSR. Because the smoothing window $U_p(\omega,\overline{\omega},h_0)$ broadens with increasing periods, as shown in Figure 5, the smoothing effect of RMHVSR becomes stronger, reducing its sensitivity to long-period signals.

To evaluate whether RMHVSR or FMHVSR provides more reasonable results, 16 sites were further analyzed based on the borehole data. Because of the lack of soil information, the No. 104 site was excluded. The site fundamental period T of the remaining sites was calculated using equation 4 (Nakamura, 1989):

$$T = 4H_1/\overline{V}_S, \tag{4}$$

in which H_1 is the total layer thickness and $\overline{V}_S$ is the average shear-wave velocity. Because the required $\overline{V}_S$ was unavailable for these sites, the N-value was converted into V_S using an empirical formula proposed by Kato and Tamori (2011) based on various soil data in Japan, expressed as

$$V_S = \alpha(N+1)^{\beta} * H_2^{\gamma} + \lambda, \tag{5}$$

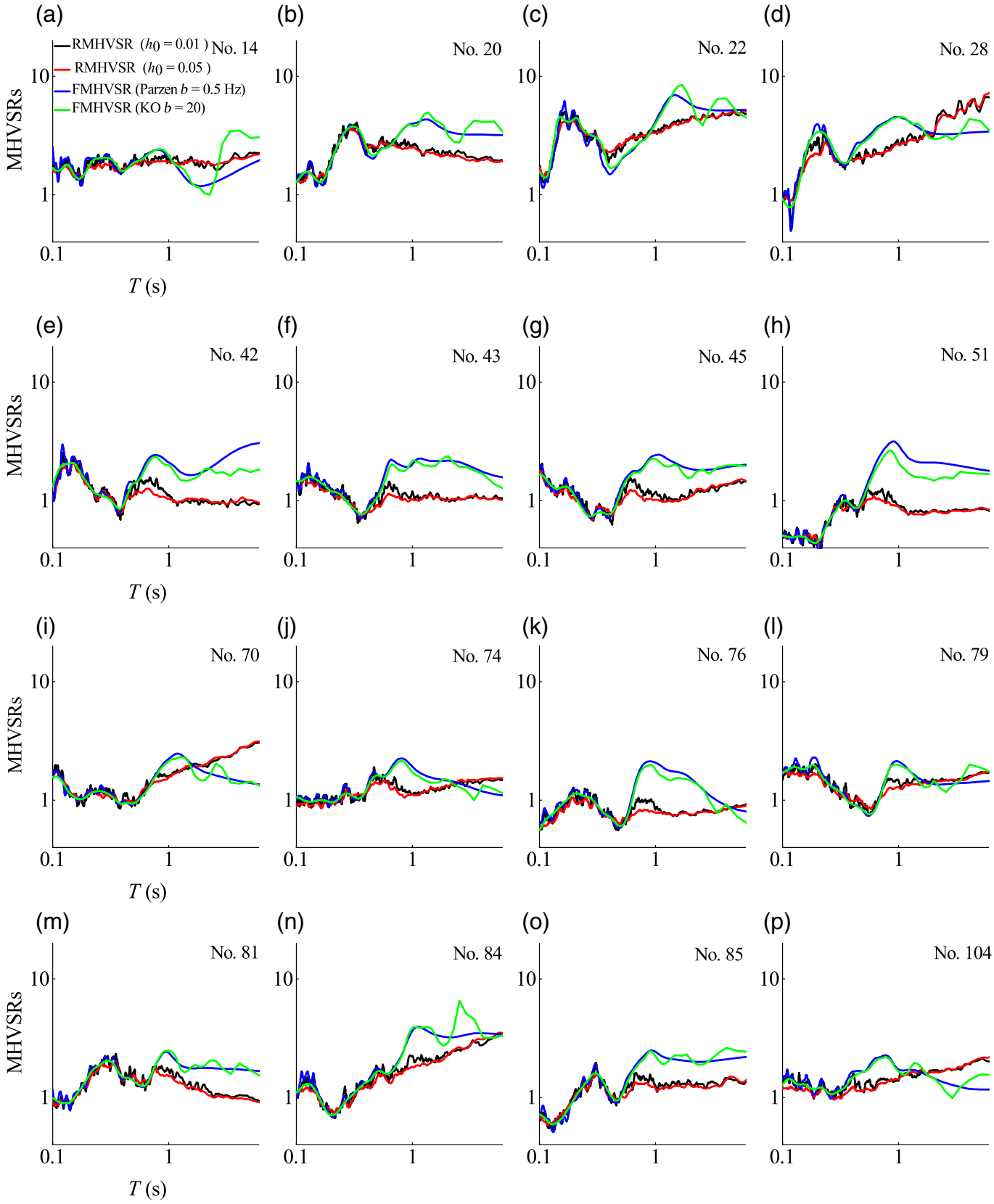

Figure 10. Comparison of RMHVSR and FMHVSR results demonstrating poor consistency, considering damping ratios of 0.01 and 0.05. For the FMHVSR results, FAS is smoothed by the Parzen window with b = 0.5 Hz and KO window with b = 20. Panels (a–p) represent the results corresponding to the site number in each figure, respectively. The color version of this figure is available only in the electronic edition.

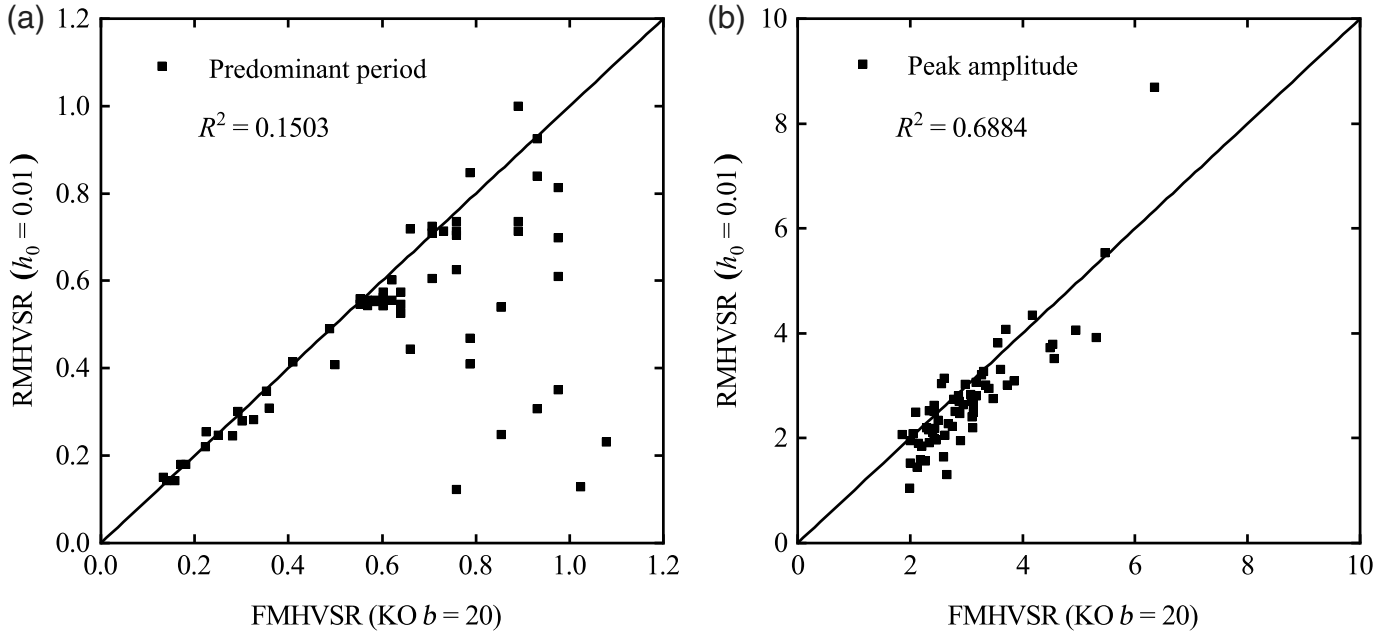

Figure 11. The correlation between the predominant period and peak amplitude of FMHVSR and RMHVSR. The FAS is smoothed using the KO window, and the response spectrum is calculated with a damping ratio of 0.01. (a) Predominant period and (b) peak amplitude.

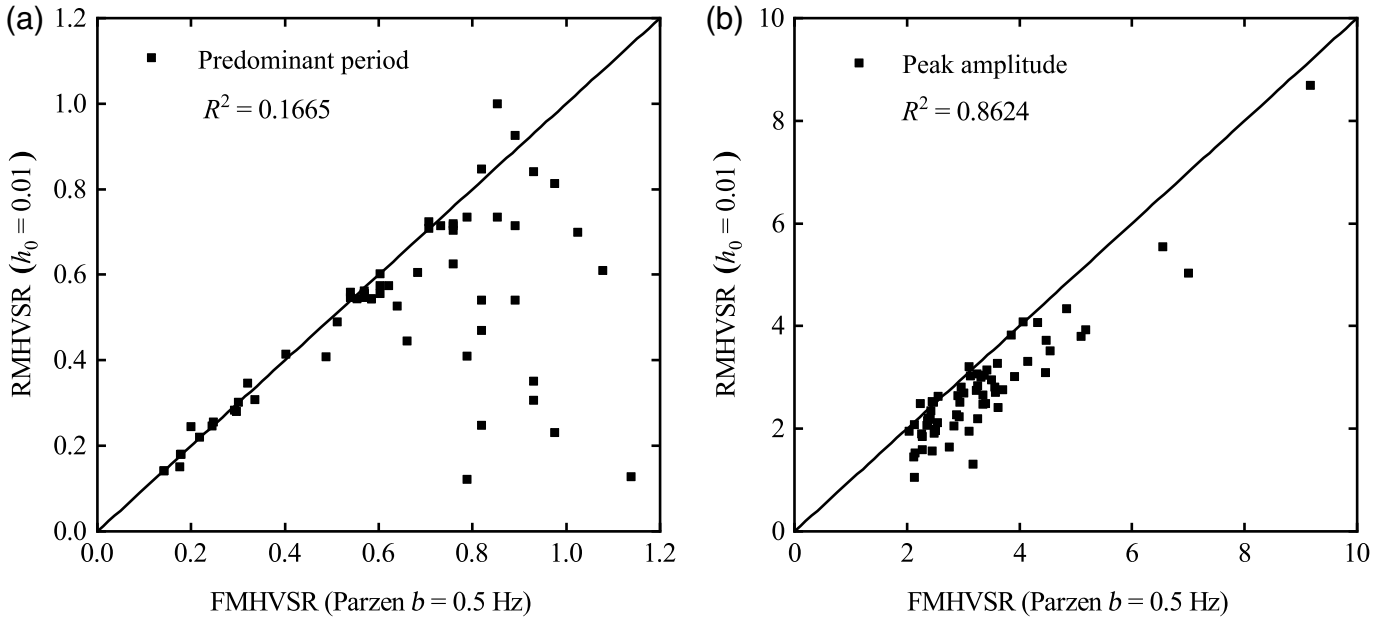

Figure 12. The correlation between the predominant period and peak amplitude of FMHVSR and RMHVSR. The FAS is smoothed using the Parzen window, and the response spectrum is calculated with a damping ratio of 0.01. (a) Predominant period and (b) peak amplitude.

in which N represents the N-value, H_2 is the depth of the N-value measurement, α, β, and γ are coefficients determined through multiple regression analysis, and λ is a constant term. Table 2 provides the regression coefficients for the V_S empirical relationship. The average shear-wave velocity $\overline{V}_S$ for each site was then obtained using the travel-time weighted average $\overline{V}_S = \left(\frac{\sum_{i=1}^{n} H_i}{\sum_{i=1}^{n} H_i / V_{S,i}}\right)$. Here, n is the total number of soil layers, i represents the ith soil layer, in which $i = 1, 2, \ldots, n$. H_i is the thickness of the ith soil layer, and $V_{S,i}$ is the shear-wave velocity of the ith soil layer. Figure 14 presents the site fundamental period T for these 15 sites.

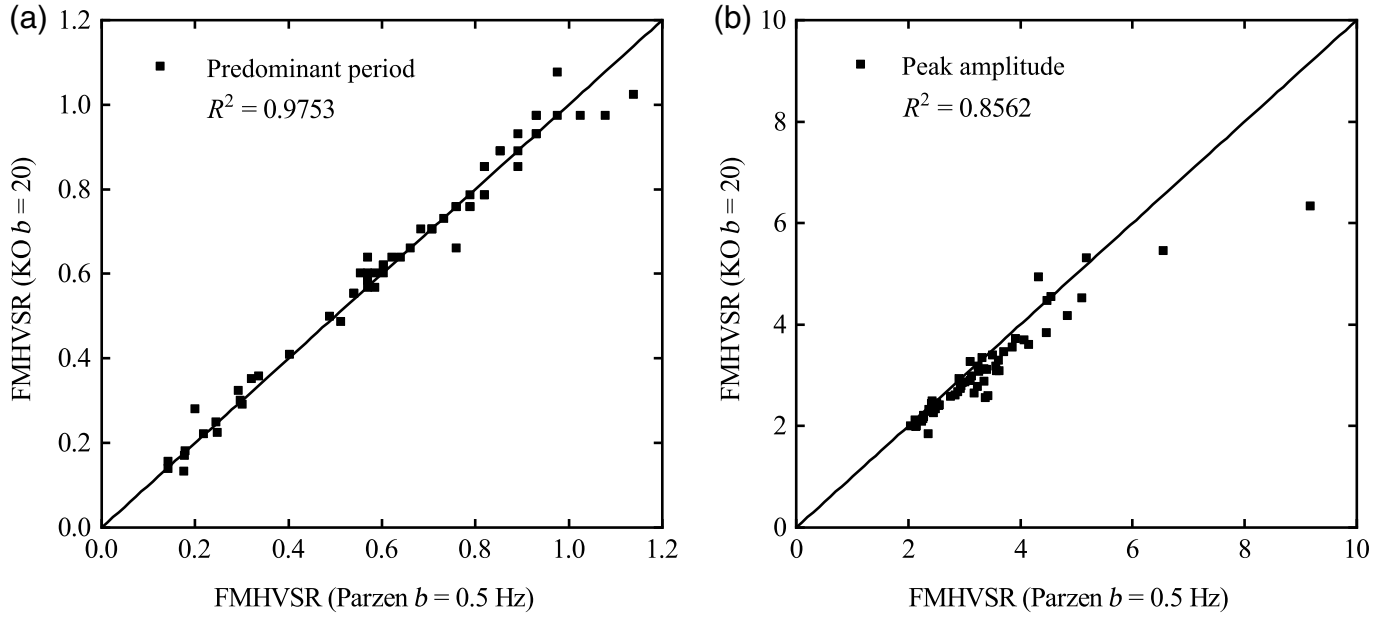

Figure 13. The correlation between the predominant period and peak amplitude of FMHVSR calculated using the KO window and Parzen window. (a) Predominant period and (b) peak amplitude.

Notably, the No. 51, No. 74, and No. 84 sites exhibit relatively high site fundamental period T-values. As shown in Figure 7, the N-values at these three sites are small and extend over significant depths: 31 m at the No. 51 site, 22 m at the No. 74 site, and 62 m at the No. 84 site, indicating that these sites consist of soft soils. These observations align with the FMHVSR results in Figure 10, in which the maximum peak appears at a long period. In these cases, FMHVSR is considered more accurate than RMHVSR. Conversely, the No. 14 and No. 22 sites exhibit relatively low site fundamental period T-values, as shown in Figure 14. From Figure 7, it can be observed that at these sites, the N-values exceed 50 within a depth of less than 10 m and extend over several meters: 15 m at the No. 14 site and 27 m at the No. 22 site. These findings indicate that these sites consist of hard soil layers, resulting in short site fundamental periods. In such cases, peaks observed in FMHVSR at longer periods can/may result from wind noise unrelated to site effects, although the average wind speed at both No. 14 and No. 22 sites during the observation period was only 2 m/s (as shown in Fig. 8). If this were the case, the long-period smoothing of the RMHVSR would tend to subdue those peaks. Consequently, the RMHVSR may provide more reliable results than FMHVSR for these sites. However, the long-period peak in the FMHVSR could also stem from other factors, such as data processing techniques. To fully determine the origin of these peaks, further investigation may be needed. For other sites with shallow boreholes, the inconsistency between RMHVSR and FMHVSR in the predominant period cannot be directly compared with the results in Figure 14. In conclusion, if the long-period peak in the FMHVSR curve is caused by noise, such as wind, RMHVSR might be more accurate than FMHVSR due to its insensitivity. However, if a source related to site effects causes a peak at a long period, RMHVSR may yield inaccurate results due to excessive smoothing.

TABLE 2
Regression Coefficient of the *S*-Wave Velocity Estimation Formula

Soil Classification	α	β	γ	λ
Alluvial cohesive	104.1	0.219	0.123	−30.2
Alluvial sandy	61.8	0.229	0.185	25.5
Alluvial gravelly	109.9	0.170	0.192	−14.3

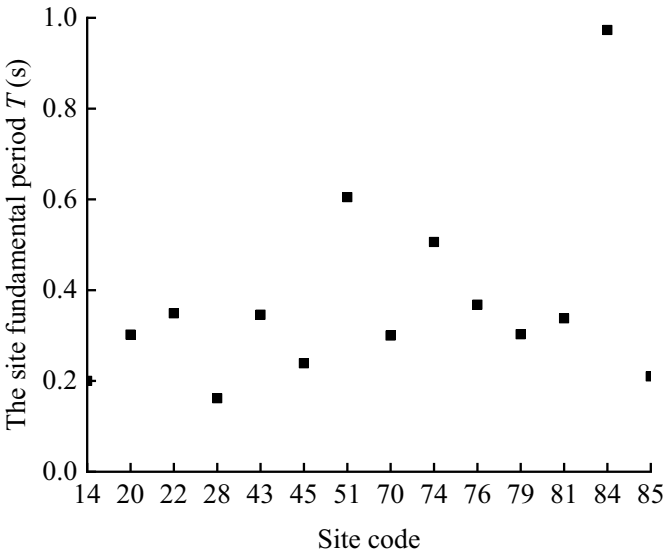

Figure 14. The site fundamental period T of 15 sites with detailed soil information.

In addition, the amplitude of the FMHVSR based on the Parzen window is higher than that of the KO window at shorter periods, as illustrated in Figure 9d,e,h–j. Conversely, at longer periods, the FMHVSR based on the Parzen window is generally lower than that of the KO window, as shown in Figure 9b,c,f,g,k. These differences are attributed to the characteristics of the two smoothing windows. As noted by Konno and Ohmachi (1998), the Parzen window's width increases with the period on a logarithmic axis, whereas the KO window maintains a constant width across all periods. At shorter periods, the Parzen window with $b = 0.5$ Hz is narrower than the KO window with $b = 20$, resulting in less pronounced smoothing. At longer periods, however, the Parzen window becomes wider than the KO window, leading to greater smoothing. Consequently, the Parzen window is less effective at smoothing shorter periods but more effective at longer periods.

CONCLUSIONS

In this study, the applicability of RMHVSR was explored. Specifically, a theoretical analysis of RMHVSR was conducted based on RVT. In addition, RMHVSR was compared with FMHVSR using microtremor records from 104 sites in Japan, supplemented by site borehole data. The main conclusions are summarized as follows:

1. RMHVSR is the smoothed form of the square of FMHVSR. As the oscillator period T_0 increases, the bandwidth of the smoothing window $U_p(\omega,\overline{\omega},h_0)$ becomes progressively wider on a logarithmic axis, resulting in a smoother RMHVSR and lower peaks with increasing periods.
2. The RMHVSR is less sensitive to long-period signals compared to FMHVSR, making it less affected by long-period noise, such as wind.
3. For sites with short fundamental periods, RMHVSR and FMHVSR exhibit similar shapes with aligned predominant periods, although the peak amplitude of RMHVSR is lower. In such cases, RMHVSR offers distinct advantages by eliminating the need for smoothing and providing unique MHVSR results, therefore it is recommended for use under these conditions.
4. For site fundamental periods exceeding ~0.8 s, RMHVSR may smooth out the peak corresponding to the fundamental period. In such cases, it is difficult to determine whether RMHVSR or FMHVSR is more appropriate before fully identifying the origin of these peaks.
5. Increasing the damping ratio broadens the bandwidth of the smoothing window, resulting in smoother RMHVSR curves.

DATA AND RESOURCES

Shear-wave velocity V_S profiles of Kyoshin net (K-NET) and Kiban–Kyoshin network (KiK-net) recording stations were downloaded from the http://www.kyoshin.bosai.go.jp (last accessed June 2024). The N-value profiles for 97 sites can be obtained from the National Geo-Information Center (NGiC) (https://ngic.or.jp/, last accessed July 2024). The maximum and average windspeeds during the measurement period can be obtained from the Japan Meteorological Agency (https://www.jma.go.jp/jma/indexe.html, last accessed July 2024). The microtremor data analyzed were collected in Japan by our team and are available from the corresponding author upon reasonable request. MATLAB (https://ww2.mathworks.cn/products/matlab.html, last accessed September 2022) was used to calculate response-spectra-based horizontal-to-vertical spectral ratio (RMHVSR) and Fourier amplitude spectra-based MHVSR, and the code is available upon request. The supplemental material includes Figures S7–S9.

DECLARATION OF COMPETING INTERESTS

The authors acknowledge that there are no conflicts of interest recorded.

ACKNOWLEDGMENTS

This study was supported by the National Key R&D Program of China (2023YFC3805100, 2023YFC3805101) and the Tohoku Chiikizukuri Kyokai, General Incorporated Association. The authors thank the Chief Editor, Associate Editor Ivan G Wong, and an anonymous reviewer for constructive comments that significantly improved the article. Funding: This study was supported by the National Key R&D Program of China (2023YFC3805100, 2023YFC3805101) and the Tohoku Chiikizukuri Kyokai, General Incorporated Association. Authors' Contributions: Yuxin Han supported conceptualization, methodology, data curation, writing of original draft, and investigation. Yan-Gang Zhao supported visualization, supervision, and writing of reviewing and editing. Haizhong Zhang supported conceptualization, data curation, methodology, software, validation, and writing of reviewing and editing.

REFERENCES

Aoi, S., T. Kunugi, H. Nakamura, and H. Fujiwara (2011). Deployment of new strong motion seismographs of K-NET and KiK-net, in *Geotechnical, Geological and Earthquake Engineering*, A. Atilla, J. J. Bommer, J. Bray, K. Pitilakis, and S. Yasuda (Editors), Vol. 12, Springer, Dordrecht, The Netherlands, 167–186.

Araque-Perez, C. J. (2024). Reevaluating soil amplification using multi-spectral HVSR technique in La Chana Neighborhood, Granada, Spain, *J. Seismol.* **28,** no. 4, 921–949, doi: 10.1007/s10950-024-10227-2.

Bao, F., Z. W. Li, D. A. Yuen, J. Z. Zhao, J. Ren, B. F. Tian, and Q. J. Meng (2018). Shallow structure of the Tangshan fault zone unveiled by dense seismic array and horizontal-to-vertical spectral ratio method, *Phys. Earth. Planet. In.* **281,** 46–54, doi: 10.1016/j.pepi.2018.05.004.

Bard, P. Y. (1999). Microtremor measurements: A tool for site effect estimation, *The Effects of Surface Geology on Seismic Motion*, Vol. 3, 1251–1279.

Bindi, D., S. Parolai, M. Enotarpi, D. Spallarossa, P. Augliera, and M. Cattaneo (2001). Microtremor H/V spectral ratio in two sediment-filled valleys in western Liguria (Italy), *Boll. Geof. Teor. Appl.* **42,** nos. 3/4, 305–315.

Brax, M., P. Y. Bard, A. M. Duval, E. Bertrand, M. E. Rahhal, R. Jomaa, C. Cornou, C. Voisin, and A. Sursock (2018). Towards a

microzonation of the Greater Beirut area: An instrumental approach combining earthquake and ambient vibration recordings, *Bull. Earthq. Eng.* **16,** 5735–5767, doi: 10.1007/s10518-018-0438-1.

Chieppa, D., M. Hobiger, F. Nagashima, H. Kawase, and D. Fäh (2023). Identification of subsurface structures using H/V curves from earthquake recordings: Application to seismic stations in Switzerland, *Pure. Appl. Geophys.* **180,** no. 3, 755–787.

Cox, B. R., T. Cheng, J. P. Vantassel, and L. Manuel (2020). A statistical representation and frequency-domain window-rejection algorithm for single-station HVSR measurements, *Geophys. J. Int.* **221,** no. 3, 2170–2183, doi: 10.1093/gji/ggaa119.

D'Amico, V., M. Picozzi, F. Baliva, and D. Albarello (2008). Ambient noise measurements for preliminary site-effects characterization in the urban area of Florence, Italy, *Bull. Seismol. Soc. Am.* **98,** no. 3, 1373–1388, doi: 10.1785/0120070231.

Delgado, J., C. Lopez Casado, J. Giner, A. Estevez, A. Cuenca, and S. Molina (2000). Microtremors as a geophysical exploration tool: applications and limitations, *Pure. Appl. Geophys.* **157,** 1445–1462.

Diagourtas, D., A. Tzanis, and K. Makropoulos (2001). Comparative study of microtremor analysis methods, *Pure. Appl. Geophys.* **158,** 2463–2479.

Fäh, D., F. Kind, and D. Giardini (2003). Inversion of local *S*-wave velocity structures from average H/V ratios, and their use for the estimation of site-effects, *J. Seismol.* **4,** no. 7, 449–467.

Gosar, A., and A. Lenart (2010). Mapping the thickness of sediments in the Ljubljana Moor basin (Slovenia) using microtremors, *Bull. Earthq. Eng.* **8,** no. 3, 501–518.

Haghshenas, E., P. Y. Bard, and N. Theodulidis (2008). Empirical evaluation of microtremor H/V spectral ratio, *Bull. Earthq. Eng.* **6,** 75–108.

Han, Y. X., Y. G. Zhao, and H. Z. Zhang (2024). Theoretical relationship between the horizontal-to-vertical response and Fourier spectral ratios of ground motions, *Soil Dynam. Earthq. Eng.* **187,** 109010, doi: 10.1016/j.soildyn.2024.109010.

Hinzen, K. G., B. Weber, and F. Scherbaum (2004). On the resolution of H/V measurements to determine sediment thickness, a case study across a normal fault in the Lower Rhine Embayment, Germany, *J. Earthq. Eng.* **8,** no. 6, 909–926.

Kato, K., and S. Tamori (2011). Proposal of empirical relation of *S*-wave velocity based on various soil data, *AIJ J. Technol. Design* **17,** no. 36, 467–471 (in Japanese).

Kawase, H., F. Nagashima, K. Nakano, and Y. Mori (2019). Direct evaluation of *S*-wave amplification factors from microtremor H/V ratios: Double empirical corrections to "Nakamura" method, *Soil Dynam. Earthq. Eng.* **126,** 105067, doi: 10.1016/j.soildyn.2018.01.049.

Konno, K., and T. Ohmachi (1998). Ground-motion characteristics estimated from spectral ratio between horizontal and vertical components of microtremor, *Bull. Seismol. Soc. Am.* **88,** no. 1, 228–241, doi: 10.1785/BSSA0880010228.

Laouami, N. (2020). Proposal for a new site classification tool using microtremor data, *Bull. Earthq. Eng.* **18,** no. 10, 4681–4704, doi: 10.1007/s10518-020-00882-4.

Marchand, P., and L. Marmet (1983). Binomial smoothing filter: A way to avoid some pitfalls of least-squares polynomial smoothing, *Rev. Sci. Instrum.* **54,** no. 8, 1034–1041.

Mascandola, C., M. Massa, S. Barani, D. Albarello, S. Lovati, L. Martelli, and V. Poggi (2019). Mapping the seismic bedrock of the Po Plain (Italy) through ambient-vibration monitoring, *Bull. Seismol. Soc. Am.* **109,** no. 1, 164–177, doi: 10.1785/0120180193.

Massa, M., C. Mascandola, C. Ladina, S. Lovati, and S. Barani (2017). Fieldwork on local-site seismic response in the Po Plain: Examples from ambient vibration array and single station analyses, *Bull. Earthq. Eng.* **15,** 2349–2366.

Matsushima, S., T. Hirokawa, F. De Martin, H. Kawase, and F. J. Sánchez-Sesma (2014). The effect of lateral heterogeneity on horizontal-to-vertical spectral ratio of microtremors inferred from observation and synthetics, *Bull. Seismol. Soc. Am.* **104,** no. 1, 381–393, doi: 10.1785/0120120321.

Miura, H., C. Gonzales, M. Diaz, M. Estrada, F. Lazares, Z. Aguilar, D. Pan, and M. Matsuoka (2023). Assessment of site amplification factors in Southern Lima, Peru based on microtremor H/V spectral ratios and deep neural network, *J. Disaster Res.* **18,** no. 4, 298–307, doi: 10.20965/jdr.2023.p0298.

Molnar, S., A. Sirohey, J. Assaf, P. Y. Bard, S. Castellaro, B. Cornou, B. Cox, B. Guillier, B. Hassani, H. Kawase, *et al.* (2022). A review of the microtremor horizontal-to-vertical spectral ratio (MHVSR) method, *J. Seismol.* **26,** no. 4, 653–685.

Nakamura, Y. (1989). A method for dynamic characteristics estimation of subsurface using microtremor on the ground surface, *QR RTRI* **30,** no. 1, 25–33.

Okada, Y., K. Kasahara, S. Hori, K. Obara, S. Sekiguchi, H. Fujiwara, and A. Yamamoto (2004). Recent progress of seismic observation networks in Japan—Hi-net, F-net, K-NET and KiK-net, *Earth Planets Space* **56,** xv–xxviii.

Pan, D., H. Miura, T. Kanno, M. Shigefuji, and T. Abiru (2022). Deep-neural-network-based estimation of site amplification factor from microtremor H/V spectral ratio, *Bull. Seismol. Soc. Am.* **112,** no. 3, 1630–1646, doi: 10.1785/0120210300.

Pan, D., H. Miura, and C. Kwan (2024). Transfer learning model for estimating site amplification factors from limited microtremor H/V spectral ratios, *Geophys. J. In.* **237,** no. 1, 622–635, doi: 10.1093/gji/ggae065.

Parolai, S., P. Bormann, and C. Milkereit (2002). New relationships between *Vs*, thickness of sediments, and resonance frequency calculated by the H/V ratio of seismic noise for the Cologne area (Germany), *Bull. Seismol. Soc. Am.* **92,** no. 6, 2521–2527, doi: 10.1785/0120010248.

Parolai, S., M. Picozzi, S. M. Richwalski, and C. Milkereit (2005). Joint inversion of phase velocity dispersion and H/V ratio curves from seismic noise recordings using a genetic algorithm, considering higher modes, *Geophys. Res. Lett.* **32,** no. 1, L01303, doi: 10.1029/2004GL021115.

Rupar, L., and A. Gosar (2020). Mapping the thickness of Quaternary sediments in the Iška alluvial fan (Central Slovenia) using microtremor method, *Acta. Geodyn. Geomater.* **17,** no. 2, 177–190.

Scherbaum, F., K. G. Hinzen, and M. Ohrnberger (2003). Determination of shallow shear wave velocity profiles in the Cologne, Germany area using ambient vibrations, *Geophys. J. Int.* **152,** no. 3, 597–612, doi: 10.1046/j.1365-246X.2003.01856.x.

Senna, S., S. Midorikawa, and K. Wakamatsu (2008). Estimation of spectral amplification of ground using H/V spectral ratio of microtremors and geomorphological land classification, *J. Jpn. Assoc. Earthq. Eng.* **8,** no. 4, 1–15 (in Japanese).

SESAME (2004). Guidelines for the implementation of H/V spectral ratio technique on ambient vibration measurements, processing and interpretation, available at http://www.samco.org/network/download_area/paper_marcellini.pdf (last accessed June 2024).

Stolte, A., L. Wotherspoon, B. Cox, C. Wood, S. Jeong, and J. Munro (2023). The influence of multiple impedance contrasts on mHVSR site period estimates in the Canterbury Plains of New Zealand and implications for site classification, *Earthq. Spectra.* **39,** no. 1, 288–309.

Suzuki, H., O. Ishitsuka, Y. Tanazawa, K. Hayashi, and K. Oota (2019). Development of portable low-cost earthquake/microtremor observation system, *Proc. of the SEGJ Conference*, Vol. 140, 217–219 (in Japanese).

Tebbouche, M. Y., D. Machane, S. Chabane, E. H. Oubaiche, A. A. Meziani, D. Ait Benamar, H. Moulouel, G. Cheikh Lounis, R. Bensalem, and A. Bendaoud (2017). Imagery of the metamorphic bedrock roof of the Sahel active fault in the Sablettes (Algiers) reclaimed area by ambient vibration HVSR, *Arabian. J. Geosci.* **10,** no. 13, 292.

Wu, H., K. Masaki, K. Irikura, and F. J. Sánchez-Sesma (2017). Application of a simplified calculation for full-wave microtremor H/V spectral ratio based on the diffuse field approximation to identify underground velocity structures, *Earth Planets Space* **69,** 1–18.

Yao, X. X., Y. F. Ren, R. Z. Wen, and J. W. Dai (2019). Some technical notes on the data processing of the spectral ratio based on the strong-motion records, in *Technology for Earthquake Disaster Prevention*, Vol. 14, 719–730 (in Chinese).

Zare, M. A., E. Haghshenas, and M. K. Jafari (2017). Interpretation of dynamic response of a very complex landslide (Latian-Tehran) based on ambient noise investigation, *Soil Dynam. Earthq. Eng.* **100,** 559–572, doi: 10.1016/j.soildyn.2017.07.006.

Zhao, J. X., K. Irikura, J. Zhang, Y. Fukushima, P. G. Somerville, A. Asano, Y. Ohno, T. Oouchi, T. Takahashi, and H. Ogawa (2006). An empirical site-classification method for strong-motion stations in Japan using H/V response spectral ratio, *Bull. Seismol. Soc. Am.* **96,** no. 3, 914–925.

Zhu, C. B., M. Pilz, and F. Cotton (2020). Evaluation of a novel application of earthquake HVSR in site-specific amplification estimation, *Soil Dynam. Earthq. Eng.* **139,** 106301, doi: 10.1016/j.soildyn.2020.106301.

Manuscript received 24 January 2025
Published online 11 June 2025